Indian Journal of Radio & Space Physics
Vol. 27, December 1998, pp. 274-284

# Algorithm for atmospheric correction of remote sensing VNIR data

Yogesh Kant & K V S Badarinath
National Remote Sensing Agency, Balanagar, Hyderabad 500 037

Received 2 March 1998; revised 3 August 1998; accepted 18 September 1998

A simple atmospheric correction method which requires inputs that are commonly available in the form of dark surfaces in blue and red region bands has been described. The method consists of an inversion algorithm based on a simplified radiative transfer model in which the characteristics of atmospheric aerosols are estimated by the use of path radiance in blue and red bands. On the basis of this information, the retrieval of true digital number (DN) values from satellite images is possible. The method can be applied to all scenes in which some dark object can be realistically supposed to be present which is practically advantageous in retrospective studies. The comparison of the values of aerosol optical thickness estimated from this method with the ground measured values showed a substantial agreement in the accuracy of the values, suggesting the possible use of the method for practical applications.

## 1 Introduction

Aerosols scatter and absorb radiation and perturb the measurement of the ground reflectances from space. Atmospheric effects reduce the contrast of satellite images. The atmospheric effects are different for different images, because the concentration and the optical parameters of aerosol particles differ significantly in space and time[1]. Atmospheric scattering and absorption depend substantially on the wavelength of the radiation and the type of the scatterers. Scattering is usually much stronger for shorter wavelengths than for longer wavelengths[2]. Due to its strong wavelength dependence, atmospheric scattering affects the classification of surface features[3] and the remote sensing of vegetation index[4,5]. However, dependence of atmospheric effect on wavelength provides a measure for determining path radiance.

Atmospheric correction techniques may be classified into either statistical or physical modelling approaches[6,7]. Statistical approaches mainly consist of histogram minimum method, regression method, the covariance method and the regression intersection method. The other methods are based on radiative transfer models, which require *in situ* field data of specific targets in the imaged scene or simultaneous measurements of parameters[8,9]. The models based on radiative transfer offer more realistic representation of atmospheric effects as compared to statistical methods by considering the wavelength dependence of path radiance. Hence, some methodology should be followed, which can compute the atmospheric corrected (true) reflectance values from the satellite image itself and from the information that is generally available in actual cases. In the present study, an inverse technique based on the simplified radiative transfer model in the atmosphere, as suggested in the literature, has been followed. It relies only on the information that is generally available in actual cases and also defines the atmospheric characteristics more objectively[10]. On the basis of presence of dark surface targets in the image scene and a combination of two bands (blue and red), the actual aerosol model is estimated through the wavelength dependence of aerosol path radiance.

## 2 Study area

In the present study, Kakinada and its surrounding areas (16° - 17°2′ N lat., and 82° 12′ - 82° 22′ E long.) in East Godavari (EG) District, Andhra Pradesh (AP), have been taken for atmospheric

corrections. The major land-use classes in the study area include agricultural areas, plantations, scrub lands, built-up lands, etc. The climate of the district is tropical in nature and mean minimum temperature varies from 15°C in the month of January to 30°C in May. The mean maximum temperature ranges from 30°C in December to 39°C in May. Relative humidity is high during January (90.4%) and February (87.2%). The average annual rainfall of the district is about 1081 mm. The major soil types include alluvial, red soils, sandy loams and sandy clays.

## 3 Methodology

### 3.1 Data sets

Landsat thematic mapper (TM) provides 30 m spatial resolution data in six spectral bands in 0.45-2.35 μm and 120 m spatial resolution data in 10.4-12.5 μm thermal IR band. Table 1 gives the spectral characteristics of TM. The satellite data pertaining to Landsat TM of 12 Oct.1988 with path/row 141/48 (satellite reference map index) of parts of E G District, AP, in digital form have been used for the present study.

### 3.2 Model description

The basic assumptions in the model are :

(i) Earth's surface has been considered to be Lambertian.

(ii) For dark surfaces, the product of fraction of upward radiation back scattered by the atmosphere to surface and the target reflectance are considered to be negligible.

(iii) Sensor is considered as the nadir viewing, so that the view angle can be taken as zero.

Table 1—Spectral band of Landsat thematic mapper (TM) (spatial resolution, 30 m)

| Band | Wavelength range μm |
|---|---|
| 1 | 0.45 - 0.52 |
| 2 | 0.52 - 0.60 |
| 3 | 0.63 - 0.69 |
| 4 | 0.76 - 0.90 |
| 5 | 1.55 - 1.75 |
| 6 | 10.4 - 12.5* |
| 7 | 2.08 - 2.35 |

* Spatial resolution, 120 m

(iv) Adjacency effects are neglected.

The radiance, $L_0(\lambda)$, recorded by a satellite sensor can be approximated to be the combination of two components – (i) the contribution $L_p(\lambda)$ from the scattering of the direct sun beam by the atmospheric constituents called path radiance, and (ii) the contribution $L_s(\lambda)$, from the radiation which is diffusely reflected by the earth surface. Landsat TM data have 30 m spatial resolution and the adjacency effect is considered to be minimal. Figure 1 shows the different contributions to the signal recorded by the sensor. Mathematically, the radiance recorded by a satellite sensor[10] is given by,

$$L_0(\lambda) = [L_p(\lambda) + L_s(\lambda)\, T_u(\lambda)]/\,[1 - sR_s(\lambda)] \quad \ldots (1)$$

where,

$L_p$ Path radiance (which is the sum of Rayleigh and aerosol path radiance)

$L_s$ Radiance of the surface (W $m^{-2}$ $\mu m^{-1}$ $sr^{-1}$)

$R_s$ Reflectance of the surface at wavelength λ

$T_u$ (λ) Beam transmittance of the atmosphere in the upward direction

$S$ Fraction of the upward radiation backscattered by the atmosphere to the surface.

For small optical thickness and/or dark surfaces, $sR_s << 1$; so this term can be neglected from Eq. (1). With this assumption, the radiance reaching the top of the atmosphere in the direction θ to the zenith can be written as

$$L_0(\lambda) = L_p(\lambda) + L_s(\lambda)\, T_u(\lambda) \quad \ldots (2)$$

The radiance, $L_0$, of a given surface recorded at the sensor can be estimated from the digital number (DN) of the image by,

$$L_0(\lambda) = \alpha(\lambda)\, DN + \beta(\lambda) \quad \ldots (3)$$

where, α and β are the calibration constants of the sensor[11].

For the atmospheric contribution, $L_p$(up), if the aerosol optical thickness is relatively small, the separability of the Rayleigh and aerosol atmospheres can be assumed[12] as

$$L_p(\lambda) = L_r(\lambda) + L_a(\lambda) \quad \ldots (4)$$

where, 'r' refers to Rayleigh contribution and 'a' to aerosol (Mie) contribution.

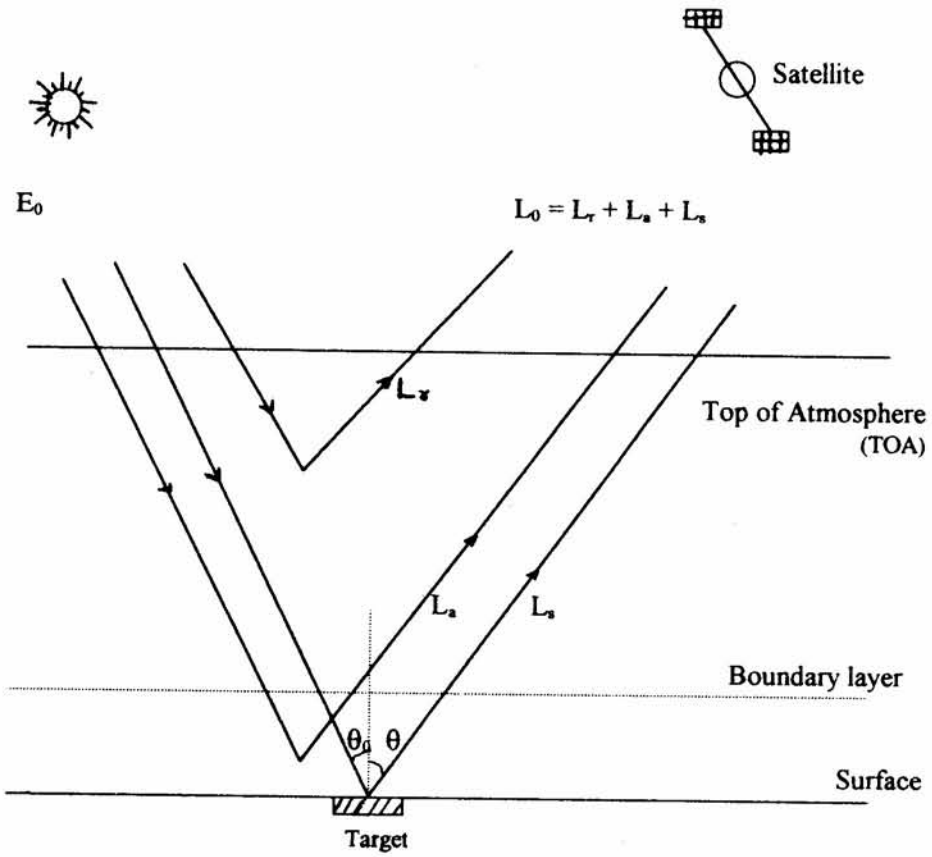


Fig. 1—Electromagnetic interactions of solar radiation in the atmosphere

The expression for the radiance of the surface will be

$$L_s(\lambda) = [L_0(\lambda) - L_p(\lambda)] / T_u(\lambda) \quad \ldots (5)$$

To obtain $L_s(\lambda)$, $L_p(\lambda)$ and $T_u(\lambda)$ need to be determined, while $L_0(\lambda)$ can be obtained from digital images. Since the dark surface objects have very low reflectance, i.e. $L_s = 0$, the dark objects radiance recorded by the sensor becomes equal to the path radiance, i.e. $L_0(\lambda) = L_p(\lambda)$, according to Eq. (5).

Thus, the path radiance can be estimated directly from the image by determining the radiance measured by the sensor over dark areas[10]. These dark areas should ideally provide zero reflectance, but owing to atmospheric effects the reflectance will have non-zero values, which is used to determine the path radiance in the present model. The dark surfaces normally correspond to water bodies in NIR region, areas in cloud's shadow (low reflectance in all bands), vegetation areas (low reflectance in blue and red regions) or to mixture of some of these factors[13].

The identification of suitable dark values is the main step in the present methodology. In this methodology, digital number (DN) over vegetation in blue and red region (dark object) has been used.

Once $L_p$(blue band) and $L_p$ (red band) from the dark objects are computed, it is possible to evaluate $L_a(\lambda)$ from Eq. (4), provided $L_r(\lambda)$ is known. Rayleigh path radiance ($L_r$) is practically constant for a particular wavelength in the atmosphere and is only dependent on the solar and view zenith angles. It can be obtained[14] for TM (blue) and TM (red) band as

$$L_r = \frac{E_0(\lambda)\cos\theta_0 P_r}{4\pi(\cos\theta_0 + \cos\theta)} \times [1 - \exp\{-\tau_r(\lambda)\,(1/\cos\theta_0 + 1/\cos\theta)\}] \times t_{uoz}(\lambda)\, t_{doz}(\lambda) \quad \ldots (6)$$

$E_0(\lambda)$ Extraterrestrial solar irradiance at wavelength $\lambda$
$\theta_0$ Solar zenith angle
$\theta$ View zenith angle (taken as 0°)
$P_r$ Rayleigh phase function
$t_{uoz}(\lambda)$ Transmittances from ozone in upward direction
$t_{doz}(\lambda)$ Transmittances from ozone in downward direction
$\tau_r(\lambda)$ Molecular optical thickness

The Rayleigh phase function is given as[15]

$$P_r = (3/4)\,[1 + \cos^2\Omega] \quad \ldots (7)$$

where, $\Omega$ is the scattering angle.

For $\theta = 0°$, $\Omega = 180 - \theta_0$.

Molecular optical thickness can be written as a function of the wavelength[16] and the height, $h_0$, of the surface above sea level[17] and is given by

$$\tau_r(\lambda, h_0) = H_r(h_0)\,[0.00859\,\lambda^{-4}\,(1 + 0.0013\,\lambda^{-2} + 0.00013\,\lambda^{-4})] \quad \ldots (8)$$

where, $\lambda$ refers to the central wavelength (in μm) of each spectral band and $H_r(h_0)$ is given as,

$$H_r(h_0) = \exp(-0.1188\,h_0 - 0.00116\,h_0^2) \quad \ldots (9)$$

Where, $h_0$ is expressed in km.

Transmittances for ozone are given as[18]

$$t_{uoz}(\lambda) = \exp[-\tau_{oz}(\lambda)] \quad \ldots (10)$$
$$t_{doz}(\lambda) = \exp[-\tau_{oz}(\lambda) / \cos\theta_0] \quad \ldots (11)$$

where, $\tau_{oz}(\lambda)$ = Optical thickness for ozone.

The relation between aerosol path radiances and the wavelength is based on radius power law distribution of particles and is given by the Angstrom formula[19]

$$L_a(\lambda) = \Gamma\,\lambda^{-\delta} \quad \ldots (12)$$

where, $\Gamma$ and $\delta$ are, respectively, related to the concentration and size distribution of particles.

It is possible to find aerosol path radiance in blue and red bands by using Eqs (3) - (6). Using $L_a$(B1) and $L_a$(B3), it is possible to calculate values of $\Gamma$ and $\delta$ for each satellite image, and then $L_a(\lambda)$ values for all band can be determined (B1 and B3 refer to blue and red bands, respectively). Thus, the optical characteristics of aerosols can be described by estimating single scattering albedo ($w_0$) and scattering phase function $P_a$ of aerosols.

The percentage of molecular atmosphere (PER) can be expressed as[20,21].

$$\text{PER} = (\lambda_1^{-\delta} - \lambda_1^{-0.8}) / (\lambda_1^{-4.08} - \lambda_1^{-0.8}) \quad \ldots (13)$$

where, $\lambda_1$ refers to the average wavelength of the spectral interval between blue and red bands, $\delta$=0.80 for a very hazy Mie atmosphere and $\delta$=4.08 for an ideal Rayleigh atmosphere.

The PER value is used to calculate a new phase function for aerosols as

$$P_a' = \text{PER} \times P_r + (1 - \text{PER}) \times P_a \quad \ldots (14)$$

where, $P_a$ is the aerosol phase function.

In this case, the two-term Henyey-Greenstein (TTHG) phase function has been applied[22,23] and is given as

$$P_a = \frac{\alpha(1-g_1^2)}{(1+g_1^2-2g_1\cos\theta_0)^{3/2}} + \frac{(1-\alpha)(1-g_2^2)}{(1+g_2^2-2g_2\cos\theta_0)^{3/2}} \quad \ldots (15)$$

where, $\alpha$, $g_1$, $g_2$ are the asymmetry factors, which strongly depend on the aerosol size distribution.

The aerosol single scattering albedo, which indicates the amount of scattering by aerosol, is given by

$$w_0 = \text{PER} \times 1.0 + (1 - \text{PER}) \times 0.90 \quad \ldots (16)$$

The values of 1.0 and 0.90 in Eq. (16), being the aerosol single scattering albedos, correspond, respectively, to an ideal Rayleigh atmosphere with non-absorbing aerosol and to a hazy atmosphere with higher proportion of absorbing aerosols in a typical agricultural environment[20].

The aerosol optical thickness can be approximated as

$$\tau_a(\lambda) = \frac{4\pi L_a(\lambda)}{E_0\,P_a'\,w_0} \quad \ldots (17)$$

The atmospheric beam transmittances can be obtained from expression,

$$T_u(\lambda) = \exp\{-\tau_{oz}(\lambda) - \tau_r(\lambda) - \tau_a(\lambda)\} \quad \ldots (18)$$

A user-friendly PC based software in 'C' language has been developed for implementing the algorithm on the satellite data. The software can be used on various satellite data sets.

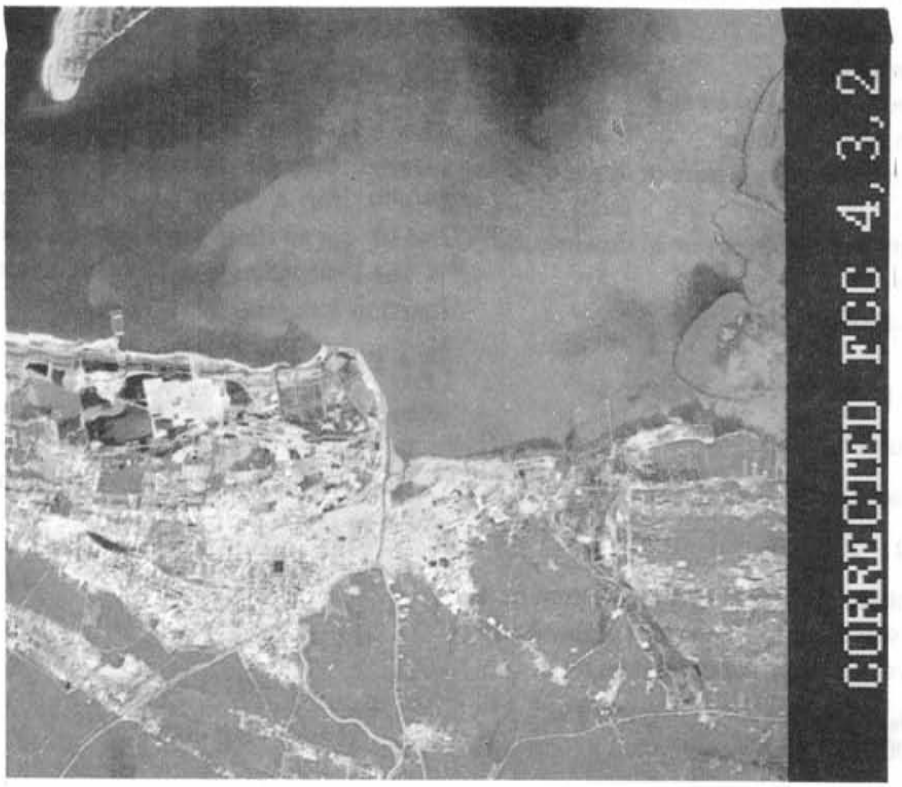


Fig. 3—Atmospheric corrected FCC of the study area (4,3,2)

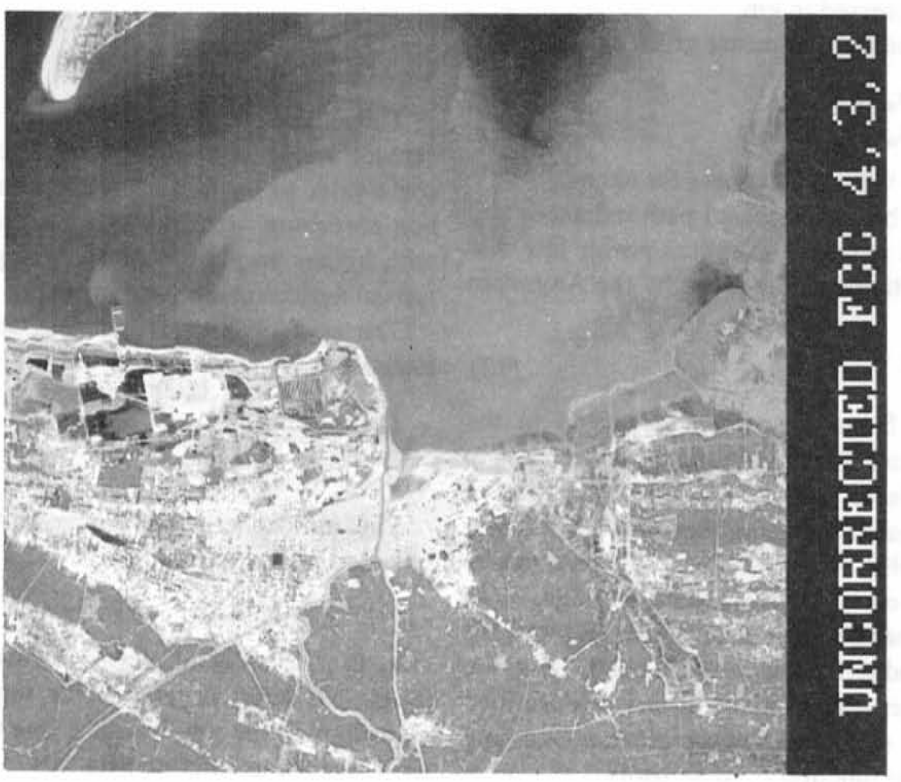


Fig. 2—False color composite (FCC) of the study area (4,3,2)

## 4 Results and discussion

The model described has been implemented on the study area shown in Fig. 2 . The method for the atmospheric correction of TM scene developed has two basic features. First, it requires only parameters which are commonly and easily obtainable, and information which is generally obtained in the image scene. Secondly, it allows not only a simple correction of the atmospheric scattering, but also the retrieval of the real DN value of the sensed image. The digital numbers of the dark pixels in blue and red band are taken from the lowest part of the histograms. The DN values obtained as the dark pixels for vegetation were 65 for blue channel and 22 for red channel. Clearly the high DN values for vegetation in blue and red channels are due to the influence of atmospheric effects, which are otherwise low in these absorption bands. Taking these DN values, the path radiance has been calculated for blue and red channels using Eq. (3). In the estimation of ozone optical thickness, 5S code[8] has been used for the tropical atmosphere corresponding to the day of satellite data acquisition. The ozone transmittance in upward and downward directions is shown in Table 2. The ozone transmittance values decrease up to 0.66 μm and increase for longer wavelengths (>0.66 μm). Rayleigh optical thickness which is a function of wavelength and height above sea level is calculated using Eq. (8). The height is included due to the fact that the density of dry atmospheric gas decreases exponentially with the increase in height. Atmospheric pressure may vary slightly in time from place to place, but it is relatively constant[16] (SD of 1%) . The Rayleigh path radiance has been estimated using Eq. (6) and it decreases with the wavelength indicating that the maximum scattering is in the visible near-infrared region (VNIR) . Taking the calculated values for $L_r$ (blue), $L_r$(red) and $L_p$(blue), $L_p$(red), the aerosol path radiances have been calculated using Eq. (4). Aerosol path radiances for all the bands have been evaluated using Eq. (12) and are found to be in descending order indicating that there will be maximum extinction in the visible part of the electromagnetic region. Another optical characteristic of aerosol, the single scattering albedo $w_0$, has been found to be 0.932 which indicates that aerosols scatter about 93% of the radiation. The aerosol phase function is calculated using Eq. (15). Because of the lack of information on aerosol type, the values $\alpha = 0.978$, $g_1 = 0.884$, $g_2 = -0.749$ have been used for a hazy atmosphere composed of continental aerosols[23]. Aerosol optical thickness ($\tau_a$) has been evaluated from Eq. (17). The optical thickness ($\tau_a$) is a measure of attenuation of radiation propagating through the atmosphere. The value decreases with the increasing wavelength with maximum attenuation in blue channel. This $\tau_a$ can be used for the purpose of evaluating the aerosol effect on remote sensing. The atmospheric corrected surface radiances for all the channels have been calculated using Eq. (5), and the false color composite (FCC) image generated after atmospheric correction is shown in Fig.3. The net atmospheric effect is positive for shorter wavelength (the atmospheric effect increases the upward radiance) and negative for longer wavelengths. This is due to the dominant role of atmospheric scattering in shorter wavelengths, and aerosol and gaseous absorption in the longer wavelengths. The performance of the atmospheric uncorrected and corrected images of red channel is shown in Figs 4 and 5, respectively, while Figs 6 and 7 represent those of blue channel, respectively. It can be noticed from Fig. 3 that after atmospheric correction there is general improvement in contrast between various features.

Table 2—Ozone transmittance values taken from different sources

| Band Landsat-5 | Central wavelength μm | Upward transmittance | Downward transmittance |
|---|---|---|---|
| 1 | 0.48 | 0.995 | 0.99 |
| 2 | 0.57 | 0.976 | 0.953 |
| 3 | 0.66 | 0.986 | 0.973 |
| 4 | 0.83 | 1.0 | 1.0 |
| 5 | 1.61 | 1.0 | 1.0 |
| 7 | 2.21 | 1.0 | 1.0 |

The important characteristics of an atmospheric correction algorithm is its ability to retrieve true DN values in an operational environment. Figure 8 shows the corrected and uncorrected DN values for selected features so as to get an idea on the extent of atmospheric correction. Figure 8 graphically represents comparisons for all bands before and after correction. Vegetation has low values in blue

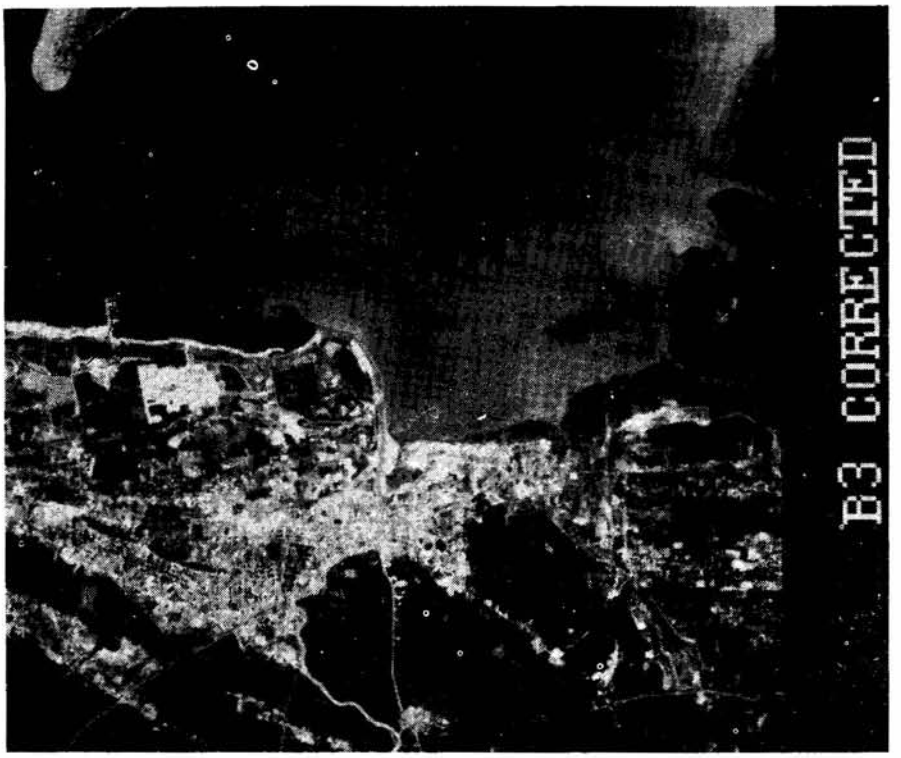


Fig. 5—Atmospheric corrected image of red band


Fig. 4—Raw digital image of red band

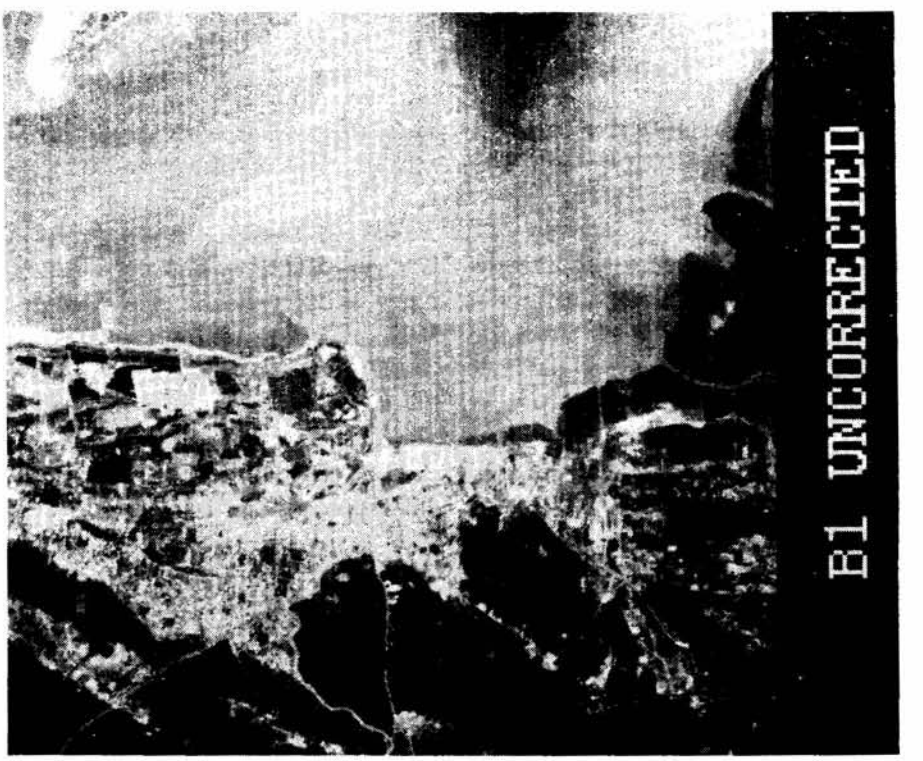


Fig. 6—Raw digital image of blue band

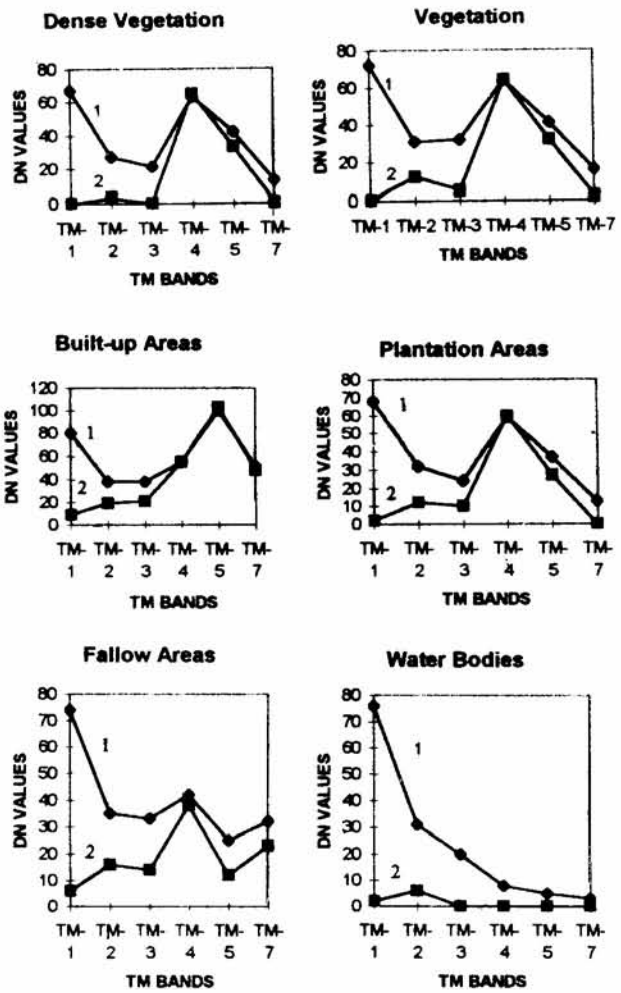


Fig. 8—Apparent DN (curve 1) and atmospheric corrected DN (curve 2) values corresponding to different site features for all TM bands

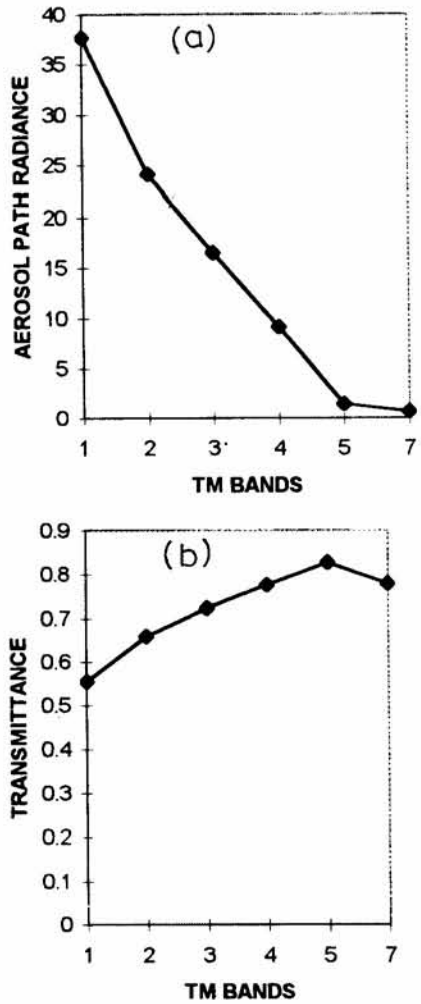


Fig. 9—Variation of (a) aerosol path radiance, and (b) upward beam transmittance with wavelength

and red after correction as compared to high values in raw data. The water bodies show a drastic improvement after atmospheric correction. In all the sample features there is a drastic improvement in visible region due to high scattering and absorption in visible region. Figure 9(a) shows the variation of aerosol path radiance with wavelength. The path radiance decreases with increasing wavelength depicting maximum absorption by aerosol in visible region. Figure 9(b) depicts the upward transmittance against wavelength. The upward transmittance is found to lie between 55% and 70% in the visible region and is greater than 75% for bands with long wavelengths indicating that TM1 (blue band) and TM2 (green band) are most strongly influenced by the atmospheric effect.

The estimated aerosol optical thickness have been compared with the nearest ground measurement at Visakhapatnam[24] collected in October 1988 and Fig. 10 (a) shows the wavelength dependence of aerosol optical thickness and Fig. 10 (b) shows the ground-based multiwavelength solar radiometer measured $\tau_a$ values. The results indicate that the aerosol optical thickness estimated from the above methodology is in reasonable agreement with the ground measured values, suggesting the possible use of the method in estimating aerosol optical thickness over the regions where no measurements are available.

## 5 Conclusions

The methodology is applicable to cases in which the presence of some non-reflective surface can be

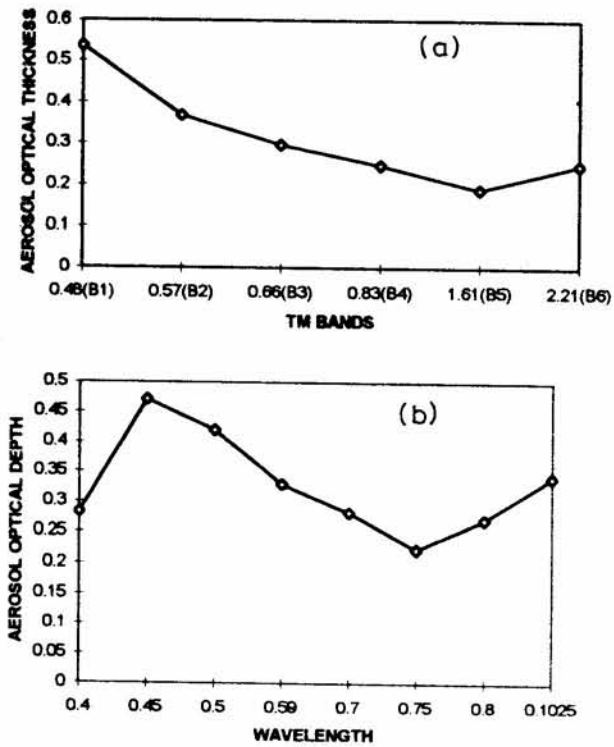


Fig. 10—(a) Model-estimated aerosol optical thickness corresponding to TM bands analysed in the study area, and (b) ground-based MWR measured aerosol optical thickness as a function of wavelength

realistically assumed. The assumptions can hold good for all the scenes taken over areas where shadows, dense vegetation, water bodies or some dark surfaces are known to be present and under clear atmospheric conditions. The performance of the method is good, which is considered acceptable for most applications. Errors are related to the selection of dark-object digital number, assumptions on the atmospheric characteristics and aerosol properties.

The advantages offered by the method are notable, especially from an operational view point. More accurate atmospheric correction methods will allow reliable research about the surface properties, particularly, in multi-temporal studies and gives the possibility of comparing the information taken from different satellites. The procedure proposed also permits the estimation of aerosol optical thickness over a region from satellite data where no ground measurements are available.

## Acknowledgements

This work has been conducted as part of ISRO-GBP programme and the authors gratefully acknowledge the support. The authors express their sincere gratitude to Prof. S K Bhan, Deputy Director and Dr D P Rao, Director, National Remote Sensing Agency, for constant encouragement and help during the course of the work. One of the authors (Y K) expresses his deep sense of gratitude to ISRO-GBP for awarding Fellowship to carry out the study.

## References

1 Putsay M, *Int J Remote Sens (UK)*,13 (1992) 1549.
2 Kaufman Y J, *IEEE Trans Geosci & Remote Sens (USA)*, 26 (1988) 441.
3 Kaufman Y J & Fraser R S , *Remote Sens Environ (USA)*, 15 (1984) 95.
4 Holben B & Fraser R S , *Int J Remote Sens (UK)*, 15 (1984) 145.
5 Tucker C J, Vanpract C, Boerwinker E & Gaston A, *Remote Sens Environ (USA)*, 13 (1983) 461.
6 Slater P N, *Optics and Optical Systems* (Addison-Wesley Publishing Company), 1980.
7 Mather P M , *Computer processing of remotely sensed image : An introduction* (Chichester : Wiley), 1987.
8 Tanre D, Deroo C, Duhaut P,Herman M, Morcrette J J, Perbos J & Deschamps P Y, *Simulation of the satellite signal in the solar spectrum (5s)*, Villeneure d'Asq France Laboratoire d'Optique Atmospherique, Universitie des Sciences et Techniques de Lille, 1986.
9 Kneizys F X, Shettle E P, Abreu L W, Chetwynd J H, Anderson G P, Gallery W O, Selby J E A & Clough S A, *User's Guide to LOWTRAN-7, AFGL-TR-88-0177*, Air Force Geophysics Laboratory, Bedford, Massachussets, USA , 1988.
10 Gilabert M A, Conese C & Maselli F, *Remote Sens Environ (USA)*, 21 (1994) 15.
11 Price J C , *Remote Sens Environ (USA)*, 21 (1987) 15.
12 Gordon H R, *Appl Opt (USA)*, 17 (1978) 1631.
13 Kaufman Y J & Sendra C, *Int J Remote Sens (UK)*, 9 (1988) 1357.
14 Saunders R W, *Int J Remote Sens (UK)*, 11 (1990) 49.
15 Schanda E, *Physics Fundamentals of Remote Sensing*, (Springer-Verlag, Berlin, Heidelberg), 1986.
16 Kaufman Y J, *In theory and Applications of Optical Remote Sensing*, edited by G Asrar (John Wiley & Sons, USA), 1989, p 336.
17 Zibordi G & Maracci G, *Int J Remote Sens (UK)*,9 (1988) 1881.
18 Sturm B, in *Remote Sensing in Meterology, Oceanography and Hydrology*, edited by A P Cracknell (Chichester: Ellis Horwood Limited), 1981, Ch 11.
19 Aranuvachapun S, *Int J Remote Sens (UK)*, 7 (1986a) 105.
20 Iqbal M, *An Introduction to Solar Radiation* (Academic

Press, New York), 1983.
21 Chahine M T, in *Manual of Remote Sensing, 2nd Edition,* edited by R N Colwell (American Society of Photogrammetry, Fall Church, Virgina), 1983, p 165.
22 Aranuvachapun S, *Remote Sens Environ (USA)*, 13 (1983) 131.
23 Liou K N , *An Introduction to Atmospheric Radiation,* (Academic Press, New York), 1980.
24 Krishna Moorthy K & Prabha R Nair , *Scientific Report, ISRO: ISRO-IMAP-SR-38 92,* 1992.